Article

Cannabidiol-loaded mixed polymeric micelles of chitosan/ poly(vinyl alcohol) and poly(methyl methacrylate) for trans-corneal delivery

Alejandro Sosnik [1,*], Ronya Ben Shabo [1] and Hen Moshe Halamish [1]

[1] Laboratory of Pharmaceutical Nanomaterials Science, Department of Materials Science and Engineering, Technion-Israel Institute of Technology, Haifa, Israel; ronyabs22@gmail.com (Ronya Ben Shabo); hen-moshe@campus.technion.ac.il (Hen Moshe Halamish)

* Author to whom correspondence should be addressed: sosnik@technion.ac.il, alesosnik@gmail.com; Tel.: +972-77-887-1971

Abstract: Ocular drug delivery is one of the most challenging administration routes due to the very low drug bioavailability. In this work, we produce and characterize mucoadhesive mixed polymeric micelles (PMs) made of chitosan and poly(vinyl alcohol) backbones graft-hydrophobized with short poly(methyl methacrylate) blocks and use them to encapsulate cannabidiol (CBD), an anti-inflammatory cannabinoid. CBD-loaded mixed PMs are physically stabilized by ionotropic crosslinking of the CS domains with sodium tripolyphoshate and spray-drying. These mixed PMs display CBD loading capacity of 20% w/w and sizes of 100-200 nm, and spherical morphology (cryogenic-transmission electron microscopy). The good compatibility of the unloaded and CBD-loaded PMs is assessed in a human corneal epithelial cell line. Then, we confirm the permeability of CBD-free PMs and nanoencapsulated CBD in cornea cell monolayers under liquid-liquid and air-liquid conditions. Overall, our results highlight the potential of these polymeric nanocarriers for ocular drug delivery.

Keywords: Polymeric micelles; cannabidiol (CBD); spray-drying; ocular drug delivery; corneal epithelial cells

1. Introduction

Cannabidiol (CBD, **Figure 1**) is one of the more than 120 phytocannabinoids produced by *Cannabis sativa* [1]. Over the last decades, cannabis has emerged as a promising therapeutic agent to treat a broad spectrum of local and systemic diseases [2,3], and the global market is expected to grow at a compound annual growth rate of ~20% and reach $82.2 billion in 2027 [4]. CBD has neuroprotective, antiemetic, antioxidant, anti-cancer and anti-inflammatory properties and it is not psychotropic (Ujváry & Hanuš 2016), which makes it appealing also for the therapy in pediatric diseases. In this context, natural and synthetic CBD has been proposed in the therapy of cancer, epilepsy, pain, inflammation and autism spectrum disorder with promising clinical results [2,3,6,7]. The development of CBD formulations is challenging because this compound is highly lipophilic (partition coefficient - log P - of 6.3) [8]. CBD is classified into Class II of the Biopharmaceutics Classification System (BCS), showing low water solubility and high permeability across biological barriers [9,10]. Oral CBD is often administered in oil or alcoholic formulations [11], and undergoes limited intestinal absorption and substantial hepatic first-pass, which results in a very low oral bioavailability (<20%) [11].

Recently, CBD has been proposed in the treatment of different degenerative and inflammatory diseases of the eye such as macular and retinal degeneration, glaucoma, and uveitis [13–17]. The local administration of lipophilic cannabinoids to the eye has been attempted with ophthalmic drops that minimize systemic side effects (Grotenhermen,

Preprints (www.preprints.org) | NOT PEER-REVIEWED | Posted: 19 November 2021 doi:10.20944/preprints202111.0364.v1

2003). However, this delivery strategy is of limited efficacy for highly hydrophobic drugs such as CBD because solubility in the aqueous lachrymal medium is critical to ensure ocular absorption. In addition, the residence time of conventional liquid formulations on the eye surface is extremely short (15-30 s) owing to lacrimation [19]. The remaining drug has to cross very dense ocular tissues such as the cornea and the conjunctiva to reach the inner layers [20–22]. Thus, the bioavailability of drugs administered by using eye drops (e.g., solutions, suspensions) is <5% of the total administered dose. In this scenario, the use of advanced drug delivery systems for ocular delivery is called.

The use of nanotechnology for the prophylaxis, diagnosis and treatment of disease has been coined nanomedicine and it has provided valuable tools to improve pharmaceutical research and development and the efficacy of a plethora of drugs [23]. The number of nanoformulations approved by the United States Food and Drug Administration (FDA) is rapidly growing [24]. Nanotechnology has been explored to increase drug dissolution rates in biological fluids (e.g., pure drug nanoparticles), to prolong the drug residence time at the administration body site, enhance drug permeability across biological barriers, and to modify their biodistribution and target specific populations in adult disease [25,26], and to a more limited extent in pediatrics [27]. Following this trend, nanocarriers have become one of the most investigated strategies to improve diagnosis and treatment of ocular diseases. They can been engineered to mucoadhere to the eye surface and prolong the drug residence time, to transiently open epithelial tight junctions and cross the corneal epithelium by a paracellular pathway [28]. The diameter of the nanocarrier has to be in the 100-500 nm range to undergo transport across mucus, and its surface charge tuned to improve retention at the administration site [29]. The cornea displays negative surface charge owing to the negatively-charged nature of the mucus, making positively-charged nanoparticles ideal for electrostatic interaction and prolonged residence time which may also improve permeability into inner eye layers.

Polymeric micelles (PMs) are nanostructures spontaneously formed by the aggregation of amphiphilic block or graft copolymers in aqueous medium above the critical micellar concentration (CMC) and display sizes between 10 and several hundreds of nanometers [30–32]. During self-assembly, the hydrophobic segments fold inwards and form the hydrophobic core that can be capitalized to encapsulate hydrophobic cargos, and increase their apparent solubility in water (Sosnik, 2013). Conversely, the hydrophilic segments fold outwards and generate the hydrophilic corona that physically stabilizes the aggregate in the dispersion medium and sometimes provides a barrier for controlled release of the cargo from the micellar core. The aggregation pattern, the shape and the structure of the PM depend on the molecular weight (MW), the hydrophilic-hydrophobic balance (HLB) and the architecture of the copolymer molecule and changes in these molecular features may lead to different micellar structures, from the typical core-corona [32,33], to flower-like [34] and multimicellar ones [35], PMs usually display good cell compatibility and biocompatibility and a highly functionalized surface area that allows an efficient interaction with surfaces and chemical modifications to improve their ability to actively target drugs to specific body sites [36]. PMs are capable of stabilizing poorly water-soluble drugs physicochemically, and they have been originally investigated to prolong the drug circulation time in the bloodstream after intravenous administration and target solid tumors by the enhanced permeation and retention effect [30]. We pioneered the application of PMs in mucosal drug delivery, including oral [37], ophthalmic [38], and intranasal administration routes [39], and stated some of the key features for the design of mucoadhesive counterparts [40]. In this framework, we produced PMs by the hydrophobization of the side-chain of mucoadhesive hydrophilic polymeric backbones of chitosan (CS) and poly(vinyl alcohol) with different hydrophobic blocks such as poly(epsilon-caprolactone), poly(*N*-isopropyl acrylamide) and poly(methyl methacrylate) (PMMA) [41–45] and used them to produce mixed PMs with optimal cell compatibility and permeability across epithelium models *in vitro* [46]. We also introduced non-covalent crosslinking and physical stabilization of PMs by using selective mild chemistries that preserve the properties of the cargo [42,43].

Preprints (www.preprints.org) | NOT PEER-REVIEWED | Posted: 19 November 2021 doi:10.20944/preprints202111.0364.v1

Aiming to improve the aqueous solubility of CBD and its transport across epithelial barriers, in this work, we initially produced and characterized mixed CS-*g*-PMMA/PVA-*g*-PMMA PM that load up to 20% w/w of CBD. Then, we assessed their cell compatibility and permeability across an *in vitro* model of human corneal epithelium.

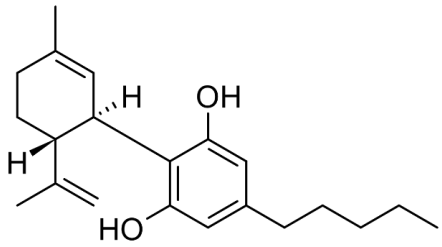

Figure 1. Chemical structure of cannabidiol (CBD).

2. Materials and Methods

2.1. Production of mixed chitosan-g-poly(methyl methacrylate):poly(vinyl alcohol)-g-poly(methyl methacrylate) polymeric micelles

The first stage was the synthesis of the CS- and PVA-based graft copolymers. CS-*g*-PMMA was synthesized by the free radical polymerization of methyl methacrylate (MMA, Alfa Aesar, Heysham, UK) in water, as described elsewhere [43,44]. For this, low MW CS (0.4 g, degree of deacetylation of 94%; viscosity of ≤100 mPa.s, MW of ~50,000 g/mol, Glentham Life Sciences, Corsham, UK) was dissolved in nitric acid 70% (0.05 M in water, 100 mL, Bio-Lab Ltd., Jerusalem, Israel) that was degassed by sonication (30 min, Elmasonic S 30, Elma Schmidbauer GmbH, Singen, Germany). Then, a tetramethylethylenediamine (TEMED, Alfa Aesar) solution (0.18 mL in 50 mL of degassed water) was poured into the CS solution and purged with nitrogen for 30 min at RT. The purged CS solution was magnetically stirred, heated to 35ºC and 0.142 mL of purified MMA pre-treated with aluminum oxide (5 g, pore size 58 Å, ~150 mesh, Sigma-Aldrich) to remove the free radical inhibitor, dispersed in degassed water (48 mL) and added to the reaction mixture. Finally, a cerium (IV) ammonium nitrate (CAN, Strem Chemicals, Inc. Newburyport, MA, USA) solution (0.66 g in 2 mL of degassed water) was added to the polymerization reaction that was allowed to proceed for 3 h at 35ºC under continuous N_2 flow. After 3 h, the polymerization was quenched by adding 0.13 g of hydroquinone (HQ, Merck GmbH, Hohenbrunn, Germany). The product was purified by dialysis against distilled water using a regenerated cellulose dialysis membrane with molecular weight cutoff (MWCO) of 12–14 kDa (Spectra/Por® 4 nominal flat width of 75 mm, diameter of 48 mm and volume/length ratio of 18 mL/cm, Spectrum Laboratories, Inc., Rancho Dominguez, CA, USA) for 48–72 h and freeze-dried (Labconco Free Zone 4.5 plus L Benchtop Freeze Dry System, Kansas City, MO, USA). The product was stored at 4ºC until use. This copolymer is named CS-PMMA30, where 30 represents the relative PMMA weight content in the copolymer (%PMMA), as determined by proton-nuclear magnetic resonance (^{1}H-NMR, see below) [43,44]. The same chemical pathway was used for the synthesis of a PVA-*g*-PMMA copolymer with a %PMMA of 16%, namely PVA-PMMA16 [45]. For this, PVA (0.4 g, Mowiol® 4–88, weight-average MW of 31,000 g/mol, 87– 89% hydrolysis, Sigma-Aldrich) was dissolved in distilled water (100 mL) at RT, and TEMED (0.18 mL in 50 mL of degassed water) was dissolved in nitric acid 70% (0.45 mL). Then, TEMED and PVA solutions were degassed by sonication for 30 min, mixed and purged with nitrogen for 30 min at RT. The solution was heated to 35ºC, and 0.142 mL of MMA pre-treated with aluminum oxide was dispersed in degassed water (48 mL) and added to the reaction mixture. Finally, a CAN solution (0.66

Preprints (www.preprints.org) | NOT PEER-REVIEWED | Posted: 19 November 2021 doi:10.20944/preprints202111.0364.v1

g in 2 mL of degassed water) was added, and the reaction allowed to proceed for 2 h at 35°C. The reaction product was purified and dried as described above, and stored at 4°C.

Reaction yields were calculated according to Eq. 1

$$\%Yield = \frac{W_{dry}}{W_{pol}+W_{PMMA}} x\ 100 \quad (1)$$

Where W_{dry} is the weight of dry copolymer (CS-PMMA30 or PVA-PMMA16) obtained after dialysis and freeze-drying, W_{pol} is the weight of the CS or PVA used in the reaction mixture, and W_{PMMA} is the weight of MMA used in the reaction. All the weights are expressed in g.

For permeability studies in cell monolayers, PVA-PMMA16 was fluorescently labeled by the conjugation of fluorescein isothiocyanate (FITC, Sigma-Aldrich) and then, used to produce mixed PMs that contain a 1:1 weight ratio of CS-PMMA30 and PVA-PMMA16 (see below). Briefly, PVA-PMMA16 (100 mg) was dissolved in 2 mL of *N,N*-dimethylformamide (DMF, Bio-Lab Ltd.) under magnetic stirring. Then, FITC was dissolved in DMF (70 mg/mL, 0.2 mL), added to the copolymer solution and the mixture stirred for 16 h protected from light, at 32°C. Finally, the product was dialyzed (48 h, regenerated cellulose dialysis membrane, MWCO of 3500 Da), freeze-dried (72–96 h) and stored protected from light at 4°C until use.

^{1}H-NMR spectra of CS-PMMA30 and PVA-PMMA16 were recorded in a 400-MHz Bruker® Avance III High Resolution spectrometer (Bruker BioSpin GmbH, Rheinstetten, Germany) and analyzed with SpinWorks 4.0 software (University of Manitoba, Winnipeg, MB, Canada). For this, we used 5% w/v solutions in deuterated dimethyl sulfoxide (DMSO-*d6*, Cambridge Isotope Laboratories, Inc., Tewksbury, MA, USA). Chemical shifts are reported in ppm using the signal of DMSO (2.50 ppm) as internal standard. Pure CS was used as control and a solution prepared in 5% w/v deuterium oxide (D_2O, Sigma-Aldrich) and trifluoroacetic acid (5% v/v, Sigma-Aldrich) because CS is insoluble in DMSO. In this case, the signal of H_2O (4.75 ppm) was used as internal standard.

To quantify the relative PMMA weight content in CS-PMMA30, a calibration curve of CS and MMA in D_2O was built using physical mixtures with different MMA:CS weight ratio (0.5–10, $R^2 = 0.9502$) that were dispersed in D_2O with 5% v/v of trifluoroacetic acid [43,44]. First, the integration of characteristic signals of each component in a physical mixture of MMA (5.8 ppm) and CS (2.8 ppm) were analyzed. For the calculation of the contribution of the H in PMMA, we calculated the intensity of one H in MMA according to the peak at 5.8 ppm that belongs to the H from the double bond of MMA and multiplied it by 3, to equal the contribution of the peaks (integrating for three H) of the methyl group of PMMA at 0.8-1.0 ppm. Thus, the ratio of the intensity of MMA:CS is based on the peak in 5.8 ppm and the peak 2.8 ppm (H-C-NH_2) in CS. In CS-*g*-PMMA30, the integration ratio was calculated using the peaks of PMMA at 0.8-1.0 ppm and of CS at 2.8 ppm. Then, the integration of ratio was interpolated in the calibration curve to determine the %PMMA [43,44].

To quantify the %PMMA in PVA-*g*-PMMA16, a calibration curve of MMA:PVA (weight ratio of 0.5-6.25, $R^2 = 0.9978$) was built in DMSO-*d6* and the ratio between the integration of the characteristic signals of PVA at 4.5 ppm (–OH pendant moieties), 3.9 ppm (–CH– of the backbone) and 1.3 ppm (–CH_2– of the backbone) and methyl group of MMA at 0.8-1.0 ppm calculated [45].

The thermal behavior of the copolymers, pure CBD and the different CBD-free and CBD-loaded PMs was analyzed by differential scanning calorimetry (DSC) in a 2 STAR^e system simultaneous thermal analyzer with STAR^e Software V13 (Metter-Toledo, Schwerzenbach,

Preprints (www.preprints.org) | NOT PEER-REVIEWED | Posted: 19 November 2021 doi:10.20944/preprints202111.0364.v1

Switzerland) with intra-cooler (Huber TC100) under dry nitrogen atmosphere (flow of 20 mL/min) and In as standard. For this, samples (5.0-15.0 mg) were sealed in 40 μL Al-crucibles pans (Metter-Toledo) and subjected to different heating-cooling cycles (10ºC/min). For CS-PMMA30, PVA-PMMA16, and the CBD-free and CBD-loaded mixed PMs, the protocol was the following: (i) cooling from 35 to -70ºC, (ii) heating from -70 to 100ºC to erase the thermal history, (iii) isothermal heating at 100ºC (30 min) to eliminate water traces, (iv) heating from 100 to 300ºC, and (v) cooling from 300 to 35ºC. For pure CBD, the protocol was (i) cooling from 35 to -70ºC, (ii) heating from -70 to 100ºC, (iii) isothermal heating at 100ºC (30 min, to eliminate water traces), and (iv) cooling from 100 to 35ºC. The glass transition temperature (T_g) and the melting temperature (T_m) of copolymers and CBD-free and CBD-loaded PMs were determined in the first heating ramp. Melting enthalpy (ΔH_m) values were normalized to the polymer weight content in the copolymer sample.

CBD-free and CBD-loaded mixed CS-*g*-PMMA30:PVA-*g*-PMMA16 (1:1 weight ratio) PMs were prepared by using a microfluidics system designed and fabricated in our laboratory [47]. The microfluidics chip is comprised of three layers: the upper and lower layers are glass-made, and the middle layer is made of a 700-μm width p-type silicon wafer (100) upon which the microfluidic channels were embedded. The width and depth of the channels are 500 μm. The lengths of the inlet and outlet channels in the Y-shaped are 10 and 8 mm, respectively. To clean the microfluidic system before use, two continuous infusion pumps (Laboratory Syringe Pump, SYP-01, MRC, Kfar Saba, Israel) were filled with 10 mL of ethanol (Gadot, Netanya, Israel), pumped, and refilled again with 10 mL of distilled water that was also pumped. For the preparation of the mixed PMs (1:1 weight ratio between the graft copolymers), 16 mg CS-PMMA30 was dissolved in water (1 mL) supplemented with 10 μL of glacial acetic acid (pH of 5.5, Gadot). In parallel, 8 mg PVA-PMMA16 solution was prepared in a solution of absolute methanol (1.5 mL, Gadot). Then, CBD (4 mg, THC Pharm GmbH, Offenbache, Germany) was dissolved in the PVA-PMMA16 methanol solution. Both solutions (CS-PMMA30 in water and CBD/PVA-PMMA16 in methanol) were magnetically stirred at RT for at least 1 h, and then mixed in 1.5:0.5 methanol:water ratio. After 10-15 min of additional magnetic stirring at RT, this solution (1 mL) and distilled water (9 mL) were loaded into two separate syringes and pumped at flow rates of 0.1 and 0.9 mL/min for the CBD/copolymers solution and water phase, respectively. The final concentration of each copolymer in the final volume was 0.04% w/v and the final CBD concentration was 0.02% w/v. These final concentrations rendered mixed PMs containing 20% w/w of CBD. For crosslinking of the mixed PMs, sodium tripolyphosphate (TPP, Sigma-Aldrich) was added to the water phase (2-3 μL of 1% w/v TPP solution per 1 mL of mixed PMs). CBD-free PMs were prepared by using the same method, though without the addition of CBD, and used as blank.

The different mixed PMs were collected in glass vials and immediately characterized by dynamic light scattering (DLS, see below). Then, they were frozen at -80ºC and freeze-dried (Labconco Free Zone 4.5 plus L Benchtop Freeze Dry System) or, conversely, spray-dried (Nano Spray Dryer Büchi B-90 HP, Büchi Labortechnik AG, Flawil, Switzerland) using an open loop configuration that is feasible for aqueous systems, inlet temperature 110ºC, 80% spraying, 30 mbar pressure, 112 kHz frequency, 90% feeding rate and 125 L/min airflow rate, yield of 45%. Dry products were stored at 4ºC until use.

2.2. Characterization of mixed chitosan-g-poly(methyl methacrylate):poly(vinyl alcohol)-g-poly(methyl methacrylate) polymeric micelles

The hydrodynamic diameter (D_h), the polydispersity index (PDI, a measure of the size distribution) and the zeta-potential (Z-potential, an estimation of the surface charge density) of 0.1% w/v PMs (fresh, and dried and redispersed) were characterized by DLS (Zetasizer Nano-ZS, Malvern Instruments, Malvern, UK) operating at a scattering angle of 173º. Each value is expressed as mean ± standard deviation (S.D.) of at least three independent samples, while each DLS or Z-potential measurement is an average of at least seven runs.

Preprints (www.preprints.org) | NOT PEER-REVIEWED | Posted: 19 November 2021 doi:10.20944/preprints202111.0364.v1

The quantification of the number of PMs per mL of suspension and the visualization of their Brownian motion was conducted by nanoparticle tracking analysis (NTA, NanoSight® NS500-Zeta HSB system with high sensitivity camera, Malvern Instruments) under scattering mode. PMs were diluted 2 to 100 times in the same medium used to prepare them to fit the measurement range of the instrument (10^7-10^9 particles/mL) and immediately measured. Experimental concentrations (particle per mL) were corrected by the dilution factor.

The morphology of the fresh CBD-free (blank) and CBD-loaded mixed PMs (0.1% w/v) before and after crosslinking was visualized by cryogenic-transmission electron microscopy (cryo-TEM). For this, mixed PMs were vitrified utilizing a controlled environment vitrification system (CEVS). In this procedure, a small sample volume (~3 μL) was placed on a carbon coated perforated polymer film supported on a 200 mesh TEM grid, mounted on tweezers, and kept at a given temperature and saturated humidity inside the CEVS. Under these conditions, the sample was turned into a thin film (preferably less than 300 nm) by blotting away excess solution with a filter paper-covered metal strip. The grid was plunged quickly into liquid ethane (-183°C) and transferred and kept in liquid nitrogen (-196°C). Finally, samples were imaged by utilizing the FEI Talos 200C High Resolution TEM (Thermo Fisher Scientific, Waltham, MA, USA) equipped with a cryo-holder (cryo-specimen holder, Gatan, Inc., Pleasanton, CA, USA) and observed at -181°C and an accelerating voltage of 120 kV.

The morphology of freeze-dried and spray-dried mixed PMs after redispersion was visualized by high resolution-scanning electron microscopy (HR-SEM, acceleration voltage of 2-4 kV, Ultraplus, Zeiss, Oberkochen, Germany). Samples were placed on top of a silicon wafer (cz polished silicon wafers <100> oriented, highly doped N/Arsenic, SHE Europe Ltd., Livingston, UK). Next, the wafer was attached to the grid using carbon-tape and additional tape was placed on its frame. At the corners of the frame silver paint (SPI# 05002-AB – Silver, SPI supplies, West Chester, PA, USA) was applied. Images were obtained without carbon coating by using In-lens detector at 3-4 mm working distance. In addition, samples of freeze-dried and spray-dried mixed PMs were also analyzed by HR-SEM.

CBD after dissolution and spray-drying was quantified by the Beam test [48,49]. Briefly, a solution of 5% w/v KOH (Bio-Lab Ltd.) in absolute ethanol (Gadot) with a pH of 12 was prepared and kept at RT until use. Then, the corresponding sample for analysis was dissolved in absolute ethanol, 5% w/v KOH solution (~250 ◎L) was added, and the sample stirred for 5 min to allow the oxidation of the extracted CBD to HU-331 and bis-HU-331. Then, the absorbance was measured at 274 nm in a Multiskan GO Microplate Spectrophotometer (Thermo Fisher Scientific Oy, Vantaa, Finland), and interpolated in a calibration curve of CBD in absolute ethanol between 0.0001% and 0.1% w/v ($R^2 = 0.9992$), treated with 5% w/v KOH and the CBD concentration calculated. Results are expressed as mean ± S.D. of at least three independent measurements.

2.3. Compatibility of mixed polymeric micelles in human corneal epithelial cells

The cell compatibility of the different mixed PMs was evaluated in the human corneal epithelial (hCEc) cell line HCE-2 [50. B1] (ATCC® CRL-11135™, ATCC®, Manassas, VA, USA). Cells were seeded on 75 cm^2 flasks pre-coated with a mixture of fibronectin (0.01 mg/mL, Biological Industries, Migdal Haemek, Israel), bovine collagen type I (0.03 mg/mL, Thermo Fisher Scientific) and bovine serum albumin (0.01 mg/mL, Sigma-Aldrich) in RPMI-1640 medium (Sigma-Aldrich). Cells were cultured in keratinocyte-serum free medium (Gibco Laboratories, Grand Island, NY, USA), supplemented with bovine pituitary extract (0.05 mg/mL, Gibco Laboratories), epidermal growth factor (5 ng/mL, Gibco Laboratories), hydrocortisone (500 ng/mL, Merck Millipore, Burlington, MA, USA), human recombinant insulin (0.005 mg/mL, Gibco Laboratories) and penicillin/streptomycin (5 mL of a commercial mixture of 100 U/mL de penicillin and 100 μg/mL streptomycin per 500

Preprints (www.preprints.org) | NOT PEER-REVIEWED | Posted: 19 November 2021 doi:10.20944/preprints202111.0364.v1

mL medium, Sigma-Aldrich), maintained at 37°C in a humidified 5% CO_2 atmosphere and split every 6-7 days. Cells were harvested by trypsinization (trypsin-EDTA 0.25%, Sigma-Aldrich) and the number of live cells quantified by the trypan blue (0.4%, Sigma-Aldrich) exclusion assay. To determine the cell compatibility of the mixed PMs, cells were seeded and cultured in pre-coated 96-well plates (1.0 x 10^4 cells/well) and allowed to attach (96 h). The sample preparation method was as follows: 1% w/v PMs freshly prepared, and freeze-dried or spray-dried and redispersed in phosphate buffered saline (PBS, Sigma-Aldrich), were diluted in culture medium to a final concentration of 0.07%, 0.1% and 0.15% w/v and incubated overnight (16 h) at 37°C. Then, the culture medium was replaced by 200 µL of micellar suspension. After 4 and 24 h, the medium was removed and fresh medium (100 µL) and sterile 3-(4,5-dimethylthiazol-2-yl)-2,5-diphenyltetrazolium bromide solution (25 µL, MTT, 5 mg/mL, Sigma-Aldrich) was added. Samples were incubated for 4 h (37°C, 5 % CO_2), the supernatant was removed, the formazan crystals dissolved with DMSO (100 µL, Bio-Lab Ltd.) and the absorbance measured at 530 nm (with reference wavelength of 670 nm) in a Multiskan GO Microplate Spectrophotometer. The percentage of live cells was estimated with respect to a control treated only with culture medium (and considered 100% viable). Since the dilutions can affect the amount of nutrients available for the cells, the culture medium of the control cells was also diluted 6.67 times in PBS to mimic the most diluted PM suspension (0.15% w/v).

2.4. Permeability of mixed polymeric micelles across a human corneal epithelium model in vitro

A permeability assay was conducted with mixed PMs in hCEc monolayers, an *in vitro* model of the human cornea [50]. For this, FITC-labeled mixed CS-PMMA30:PVA-PMMA16 PMs (a stock 0.1% w/v dispersion prepared in water supplemented with acetic acid of pH 5.5) were diluted in transport medium (Hank's Balanced Salt Solution, HBSS, Sigma-Aldrich) buffered to pH 7.4 with 4-(2-hydroxyethyl)-1-piperazineethanesulfonic acid (25 mM, HEPES, Sigma-Aldrich) and $NaHCO_3$ (0.35 g/L, Sigma-Aldrich) to the final concentration (0.01% and 0.03% w/v). For this, mixed PMs were prepared with a CS-PMMA30:FITC-labeled PVA-PMMA16:PVA-PMMA16 weight ratio of 1:0.4:0.6. Fluorescently-labeled mixed PMs that were spray-dried and redispersed in HBSS were also used. For non-covalent crosslinking, a 1% w/v TPP solution in HBSS was prepared and 3 µL of TPP solution per 1 mL of PM dispersion was added at least 6 h before the permeability experiment.

Experiments were performed 14–21 days post-seeding of hCEc (4.55 x 10^5 cells/well) on cell culture inserts (ThinCert™, culture surface of 113.1 mm^2, 3.0 µm pore size, Greiner Bio-One GmbH, Frickenhausen, Germany) maintained in 12-well plates (15.85 mm diameter, 16.25 mm height, Greiner CELLSTAR, Monroe, NC, USA) with 0.5 and 1.5 mL of keratinocytes serum-free medium (see above for culture of hCEc), to the apical and basolateral, respectively. The culture medium was replaced every 2-3 days and the integrity of the hCEc monolayer was characterized by transepithelial electrical resistance (TEER) measurements performed with an epithelial volt-ohm-meter EVOM2 (WPI, Sarasota, FL, USA).

In the eye, the corneal epithelium is exposed to air. Thus, the permeability assay was conducted in two corneal epithelium models with different interface, namely air-liquid (AL) and liquid-liquid (LL) interface. In this framework, eight days after culture, inserts were either lifted to obtain an AL culture or left in culture medium to get a LL one and cultured for 1-2 more weeks. For these experiments, only inserts where the TEER was higher than 140 Ω·cm^2 were used. At the beginning of the experiment, the medium in the apical (0.5 mL) and basolateral (1.5 mL) compartments was replaced with transport medium (HBSS) without PMs and the cells incubated for 20 min at 37°C in a humidified 5% CO_2 atmosphere to enable their adjustment to the new medium. Then, transport medium in the donor (apical) compartment was replaced by the corresponding sample (0.4 mL) containing the PMs and in the acceptor compartment by fresh transport medium (1.2 mL). Plates were incubated on an orbital shaker (MRC Ltd., Holon, Israel) at 37°C and gently shaken to minimize

Preprints (www.preprints.org) | NOT PEER-REVIEWED | Posted: 19 November 2021 doi:10.20944/preprints202111.0364.v1

the impact of the unstirred water layer. After 5, 10, 15, 30, 45, 60, 90, 120, 180, and 240 min, 600 µL of medium was extracted from the acceptor compartment and replaced by the same volume of fresh transport medium to maintain the total volume in the chamber constant. The extracted medium was used for quantification of the transported PMs by fluorescence spectrophotometry in a Fluoroskan Ascent Plate Reader (Thermo Fisher Scientific Oy) using black 96-well flat bottom plates (Greiner Bio-One, Kremsmunster, Austria) at wavelengths of 485 nm for excitation and 538 nm for emission according to a calibration curve of non-crosslinked and crosslinked PMs in HBSS in a concentration range between 0.0001% and 0.1% w/v (R^2 = 0.9916 and 0.9913, respectively). The apparent permeability (P_{app}) was calculated according to Eq. 2

$$P_{app} = \frac{dc}{dt} \cdot \frac{1}{A \cdot C_0} \; [cm \cdot s^{-1}] \quad (2)$$

Where dc/dt is the permeability rate (expressed in µg/s) across the monolayer, C_0 is the initial concentration in the donor compartment (expressed in µg/cm^3), and A is the surface area of the membrane (1.131 cm^2). Results are expressed as mean ± S.D. of at least three independent experiments.

In addition, the size of the PMs in the donor and acceptor chambers before and after the experiment was measured by DLS, as described above.

At the end of each experiment (240 min), 50 µL was also removed from the donor compartment to calculate the mass balance by fluorescence spectrophotometry (see above). The percentage of PMs retained by the cell monolayer (%PMs inside cells) was estimated according to Eq. 3

$$\%\text{PMs inside cells} = 100\% - \%\text{Final donor} - \%\text{Final acceptor} \quad (3)$$

Where 100% is the total percentage of PMs at the beginning of the experiment, %Final donor is the percentage of PMs that remained in the donor compartment at the end of the experiment (4 h), and %Acceptor is the percentage of PMs that crossed to the acceptor compartment during the experiment until the end time point of 4 h. Results are expressed as mean ± S.D. of at least three independent experiments.

We also measured the permeability of CBD-loaded PMs by tracking the growing CBD concentration in the acceptor compartment over time by the Beam test (see above). For this, fresh CBD-loaded mixed PMs were prepared as described above in HBSS instead of water without any fluorescence labeling of the copolymer. Briefly, 0.1% w/v CBD-loaded PMs (20% w/w loading) were diluted to 0.03% w/v copolymers final concentration (CBD final concentration of 20% w/w in the PMs), and the permeability assay was conducted under AL and LL setups. After 5, 10, 30, 60, 90, 120, 180, and 240 min, 600 µL of medium was extracted from the acceptor compartment and replaced by the same volume of fresh transport medium to maintain the total volume in the chamber constant. The extracted medium was used for quantification of the transported CBD-loaded PMs by diluting them with ethanol (2 mL) to extract CBD and conducting the Beam test for which a CBD calibration curve in ethanol in a concentration range between 0.0001% and 0.1% w/v (R^2 = 0.9992) was built. At the end of the experiment (240 min), 50 µL was also removed from the donor side of each sample to calculate the mass balance, as described above. Results are expressed as mean ± S.D. of at least three independent experiments.

2.5. Statistical Analysis

Statistical analysis of the different experiments was performed by t-test on raw data (Microsoft Excel, Microsoft Office 2019, Microsoft Corp., Seattle, WA, USA). P-values of less than 0.05 were considered as statistically significant.

 doi:10.20944/preprints202111.0364.v1

3. Results and Discussion

3.1. Rationale

Mucoadhesive polymers have been investigated in the development of advanced local and trans-mucosal drug delivery systems [29]. CS is a polycationic natural polysaccharide of glucosamine repeating units with pendant primary amine groups that are protonated at pH <5.8 [51]. CS promotes mucoadhesion in different mucosal tissues including the corneal epithelium [52,53]. In addition, CS favors the absorption of nanoparticles by the paracellular route by transiently opening tight junctions in different epithelia [54], including the corneal epithelium [55]. CS-*N*-acetylcysteine (Lacrimera®) eye drops have been developed as a medical device and clinically trialed for the treatment of dry eye with promising results [56]. PMs can also cross epithelia by transcellular mechanisms [57]. CS emerged as a promising component to develop amphiphilic nanoparticles (e.g., PMs) that exploit this pathway [43]. CS slowly degrades in the biological tissues, mainly by the activity of lysozyme and human chitinases [58].
PVA is a synthetic water-soluble polymer broadly used in a wide range of food, biomedical and pharmaceutical applications with very good biocompatibility [59]. PVA contains hydroxyl groups that enable the interactions with the mucin by H bonding [29]. The mucoadhesive strength of PVA is 5.11 N/cm^2 [60], and greater than that of CS (0.58 N/cm^2) [54].

CS is highly positively-charged under physiological conditions, and cell toxicity has been associated with its electrostatic interaction with the negatively-charged cell membrane. However, its cell compatibility can be improved upon partial neutralization of the positive charges by ionotropic crosslinking with polyanionic molecules such as TPP, by decreasing the degree of deacetylation or by chemically modifying or mixing it with other polymers that reduce the availability of cytotoxic free primary amine groups on the nanoparticle surface [61,62]. We improved the compatibility of amphiphilic CS-*g*-oligo(*N*-isopropylacrylamide) and CS-*g*-PMMA PMs in different cell types by crosslinking them ionotropically [35,43], and by developing mixed amphiphilic counterparts with PVA-*g*-PMMA [46]. These mixed nanoparticles capitalize on advantageous properties of both hydrophilic components such as mucoadhesion, opening of epithelial tight junctions, good encapsulation capacity of PMMA for different hydrophobic cargos and cross epithelial models *in vitro* [46,63].

In this conceptual framework, we anticipated the potential of mixed CS-*g*-PMMA and PVA-*g*-PMMA PMs produced by the co-micellization to encapsulate CBD for trans-corneal delivery. The use of PMMA was supported by its broad use as pharmaceutical excipient in oral drug delivery systems [64,65] and in permanent biomedical implants such as intraocular lenses, bone cements, and fixation and other orthopedic devices [66–68]. Short PMMA blocks bound to hydrophilic backbones are expected to undergo excretion by renal filtration.

3.2. Production and characterization of CBD-loaded mixed polymeric micelles

Initially, we synthesized CS-*g*-PMMA and PVA-*g*-PMMA copolymers by the free radical graft polymerization of MMA onto the backbone of both CS and PVA, respectively (**Figure S2**). The copolymers were characterized by ^{1}H-NMR by building calibration curves with MMA:CS or MMA:PVA physical mixtures with different weight ratios, calculating the ratio between the characteristic peaks of both components and interpolating the ratio in the copolymers in the calibration curve to determine the %PMMA that was 30% and 16%, respectively. The copolymers are named CS-PMMA30 and a PVA-PMMA16. Calculated yields were ~70% and ~75% for CS-PMMA30 and PVA-PMMA16, respectively.

Preprints (www.preprints.org) | NOT PEER-REVIEWED | Posted: 19 November 2021 doi:10.20944/preprints202111.0364.v1

Thermal analysis of the two graft copolymers used to produce the mixed PMs was conducted to later assess the properties of CBD before and after nanoencapsulation. Pure CS and PVA were analyzed for comparison. Pure CS exhibited an exothermic peak starting at 230ºC due to thermal decomposition (**Figure S3**), in good agreement with the literature [69,70]. The T_g and T_m of PVA was detected at 78 and 196ºC (ΔH_m =28.8 J/g), respectively [71]. When the graft copolymers were analyzed, CS-PMMA30 exhibited only one distinctive exothermic peak of CS decomposition at ~240ºC and PVA-PMMA16 displayed T_g at 87ºC and T_m at 179ºC (ΔH_m = 24.2 J/g). In both copolymers, thermal transitions of PMMA blocks could not detected (**Figure S3**).

PMs can be produced by different methods such as simple dissolution and organic solvent diffusion and evaporation [72]. In this work, the mixed PMs were prepared by a solvent casting method in a microfluidics device [47] and their D_h, PDI, Z-potential and concentration were measured by DLS and NTA at 25 and 37ºC. In addition, NTA was used to visualize their Brownian motion in suspension. The D_h of the PMs ranged between 96 ± 6 nm for CBD-free non-crosslinked to 151 ± 8 nm for CBD-loaded crosslinked ones (**Table 1**). Temperature changes had negligible effect on the micellar size. Generally, non-crosslinked PMs, loaded or unloaded with CBD were smaller than the crosslinked counterparts, suggesting that the ionotropic crosslinking results in an enlargement of the PMs by bridging them through electrostatic interactions. Crosslinking also resulted in the reduction of the Z-potential because the charge of the amine group in the TPP-amine complexes is partially neutralized. When comparing non-crosslinked with crosslinked PMs, crosslinking only very slightly reduces the Z-potential from +38 mV to +33-35 mV, without dramatic changes in the PDI value (**Table 1**). These findings indicated that the aggregation pattern was not dramatically affected by the crosslinking. Moreover, PMs showed a slight size growth upon CBD nanoencapsulation though without affecting the PDI or the surface charge.

NTA was used to measure the D_h and concentration of the PMs and visualize them in suspension. According to NTA, the D_h of the PMs ranges between 100 and 180 nm. The same changes in the size of the PMs upon crosslinking or CBD encapsulation were observed by both techniques. At 37ºC, the size of the PMs measured by NTA increased, along with a slight decrease in the PM concentration. This behavior might stem from a slightly different co-micellization pattern of the copolymers at this T, and especially in the presence of CBD. This size growth upon heating could not be detected by DLS, which exhibits lower size resolution than NTA [73]. Representative snapshots of the visualization of different PMs in suspension by NTA are presented in **Figure S4**.

Preprints (www.preprints.org) | NOT PEER-REVIEWED | Posted: 19 November 2021 doi:10.20944/preprints202111.0364.v1

Table 1. Hydrodynamic diameter (D_h), polydispersity index (PDI), Z-potential and concentration of CBD-free and CBD-loaded mixed PMs (0.1% w/v) before and after TPP crosslinking, as measured by DLS and NTA.

Sample	Temperature (ºC)	DLS			NTA	
		D_h – Intensity (nm) ± S.D.	PDI ± S.D.	Z- potential (+mV) ± S.D.	D_h (nm) ± S.D.	Concentration (*10^9 particles/mL) ± S.D.
Non-crosslinked mixed PMs	25	100 ± 10	0.30 ± 0.07	+38 ± 2	114 ± 3	9.5 ± 0.3
	37	96 ± 6	0.32 ± 0.07	+33 ± 3	133 ± 1	3.9 ± 0.3
Crosslinked mixed PMs	25	140 ± 20	0.38 ± 0.05	+34 ± 4	129 ± 2	9.7 ± 0.4
	37	140 ± 10	0.31 ± 0.07	+32 ± 4	144 ± 4	3.6 ± 0.2
CBD-loaded non-crosslinked mixed PMs	25	144 ± 6	0.21 ± 0.02	+35 ± 2	151 ± 1	9.6 ± 0.1
	37	142 ± 9	0.19 ± 0.02	+33 ± 1	196 ± 2	3.4 ± 0.2
CBD-loaded crosslinked mixed PMs	25	147 ± 9	0.19 ± 0.03	+34 ± 3	120 ± 4	9.0 ± 0.7
	37	151 ± 8	0.17 ± 0.02	+33 ± 3	177 ± 4	3.9 ± 0.1

CBD can degrade upon exposure to temperature >37°C and especially light [74]. CBD could also undergo auto-oxidation [75]. For example, Δ^9- and Δ^8-tetrahydrocannabinol impurities were detected in pure CBD samples stored in the darkness at RT for three months [76]. Since CBD is highly lipophilic, it is usually dissolved in oily solvents that might undergo oxidation and trigger its oxidation.

DSC is useful to characterize the crystallinity or amorphousness of pure drugs and polymers, and their combinations. We comparatively assessed the thermal properties of pure CBD, and CBD-free and CBD-loaded mixed PMs. Pure CBD showed T_m at ~70°C (ΔH_m = 68.3 J/g) [77], while CS-PMMA30:PVA-PMMA16 physical mixtures (1:1 weight ratio) without and with 20% w/w CBD showed a broad exothermal peak in the 240-270°C range associated with CS decomposition (**Figure 2**). In addition, the T_m of crystalline CBD in the physical mixture could be detected.

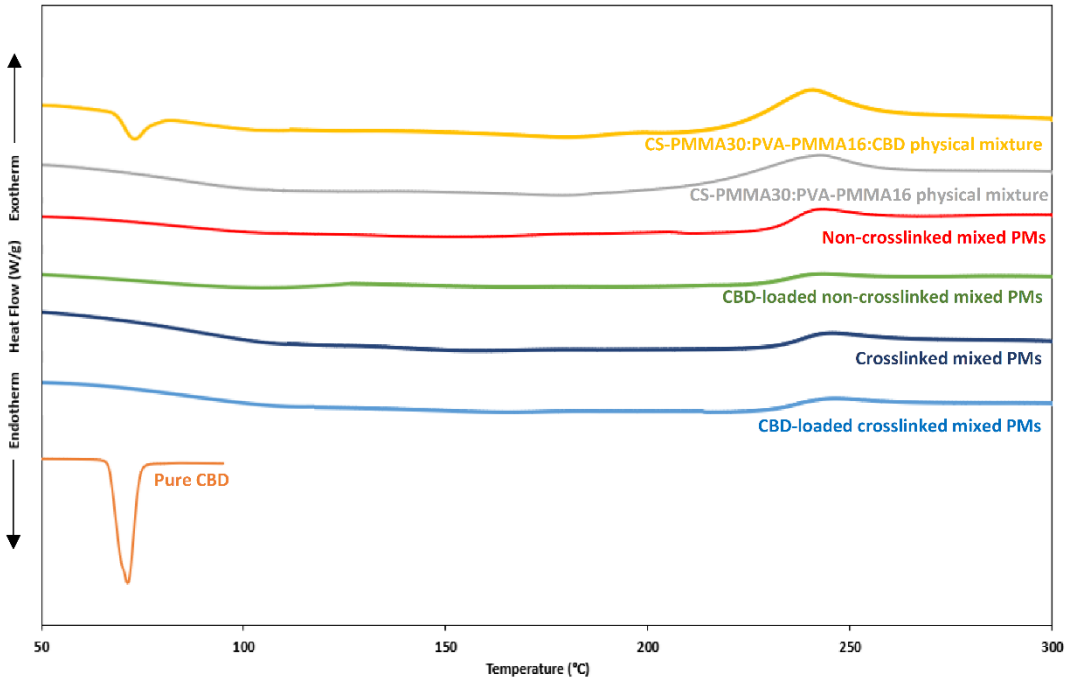

Figure 2. DSC thermograms of pure CBD, physical mixtures of copolymers without and with CBD and CBD-free and CBD-loaded spray-dried mixed PMs, as measured by DSC. The weight ratio in the CS-PMMA30:PVA-PMMA16 and CS-PMMA30:PVA-PMMA16:CBD physical mixtures was 1:1 and 1:1:0.5, respectively.

We also analyzed the thermal behavior of mixed PMs (non-crosslinked and crosslinked and CBD-free and CBD-loaded) after spray-drying. Since the crosslinking with TPP is not covalent, we did not expect to observe major differences between non-crosslinked and crosslinked PMs by DSC. The DSC thermogram of mixed PMs was a combination of those of the individual components, though the T_m of PVA was not detected in the mixed PMs, indicating that it is amorphous (**Figure 2**).

Drugs nanoencapsulated within hydrophobic polymeric nanoparticles are usually amorphous owing to the formation of solid solutions. The absence of a CBD melting endotherm in CBD-loaded PMs confirmed that this compound is amorphous (**Figure 2**). As mentioned above, CBD could undergo thermal degradation. Since some mixed PMs were spray-dried at relatively high temperature (105°C), we wanted to ensure that the encapsulated CBD does not undergo thermal decomposition. The Nano Spray Dryer B-90 HP is expected to minimize the exposure of active molecules to the heat to a fraction of second

Preprints (www.preprints.org) | NOT PEER-REVIEWED | Posted: 19 November 2021 doi:10.20944/preprints202111.0364.v1

and thus, prevent their thermal decomposition [78]. However, the stability of each compound might change. Therefore, we dissolved pure CBD in absolute ethanol, at the final concentration obtained after the encapsulation process (0.02% w/v) and spray-dried it under the same conditions used for the mixed PMs. Then, spray-dried pure CBD was collected, and Beam test was conducted on three samples. The CBD content in the spray-dried samples was 98.5%, indicating that CBD withstands the spray-drying conditions.

The spherical morphology of the CBD-free and CBD-loaded mixed PMs was visualized by cryo-TEM (**Figure 3**). Non-crosslinked mixed PMs showed a smaller diameter (70-90 nm) than crosslinked ones (100-120 nm for CBD-free PMs and 120-170 nm for CBD-loaded PMs). As expected, the diameter was smaller than that D_h measured by DLS and NTA because the latter methods measure the hydrodynamic size that comprises also hydration water.

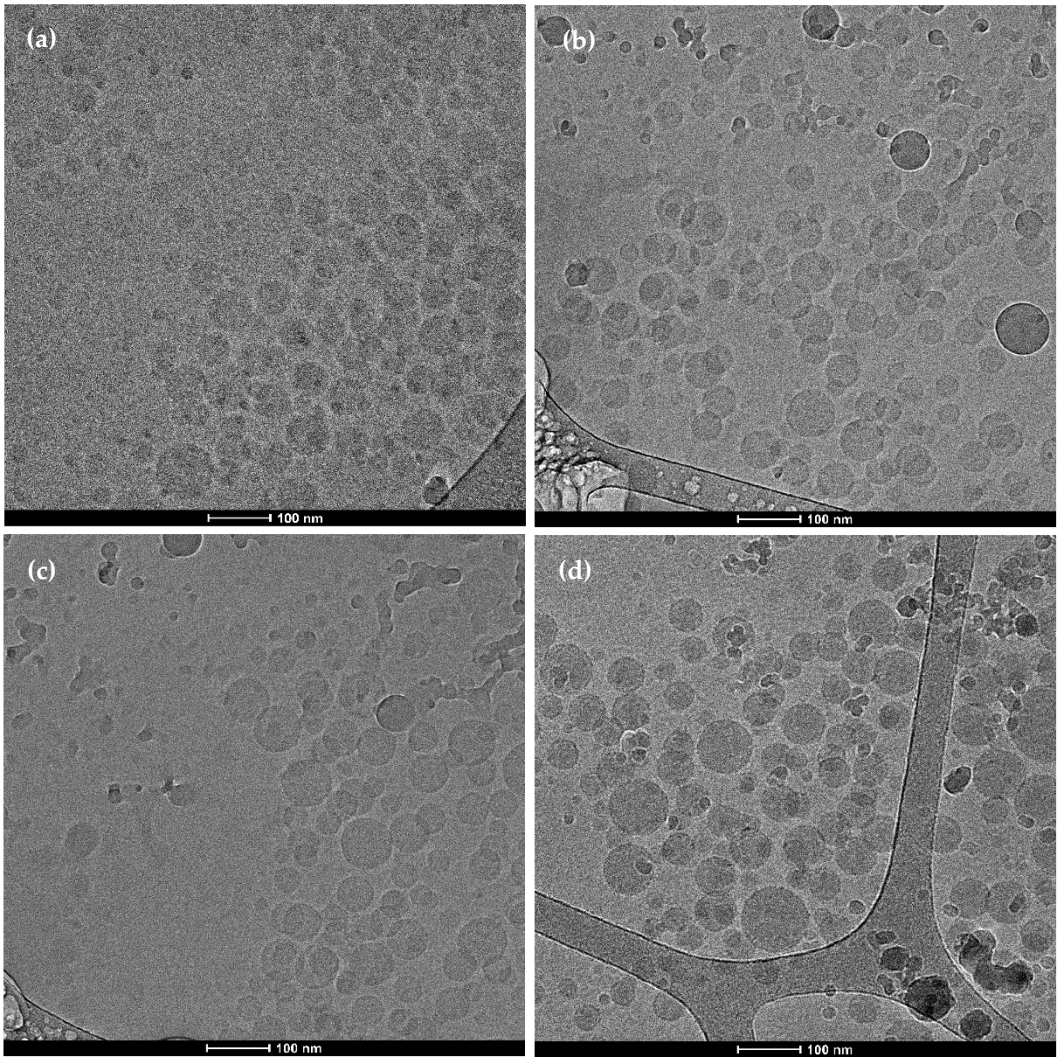

Figure 3. Representative cryo-TEM micrographs of fresh (A) CBD-free non-crosslinked mixed PMs, (B) CBD-free crosslinked mixed PMs, (C) CBD-loaded non-crosslinked mixed PMs, and (D) CBD-loaded crosslinked mixed PMs.

3.3. Drying and redispersion of CBD-loaded mixed polymeric micelles

Preprints (www.preprints.org) | NOT PEER-REVIEWED | Posted: 19 November 2021 doi:10.20944/preprints202111.0364.v1

Drying methods such as freeze-drying have been investigated to improve the long-term physicochemical stability of nanoformulations. In the case of the freeze-drying of nanoparticles (the most popular in the pharma industry), the addition of cryo/lyoprotectants in relatively large relative amounts is often required to preserve their original size upon redispersion [79]. Otherwise, nanoparticles might undergo irreversible agglomeration. In recent years, spray-drying has gained interest because additives are not needed [78]. In this context, CBD-free and CBD-loaded mixed PMs before and after crosslinking were freeze-dried and spray-dried and the morphology of the dry powders analyzed by HR-SEM. In addition, dry powders were redispersed in the original volume in water and characterized again by DLS.

Freeze-dried non-crosslinked mixed PMs were rounded and in the nanometer scale range (**Figure 4**).

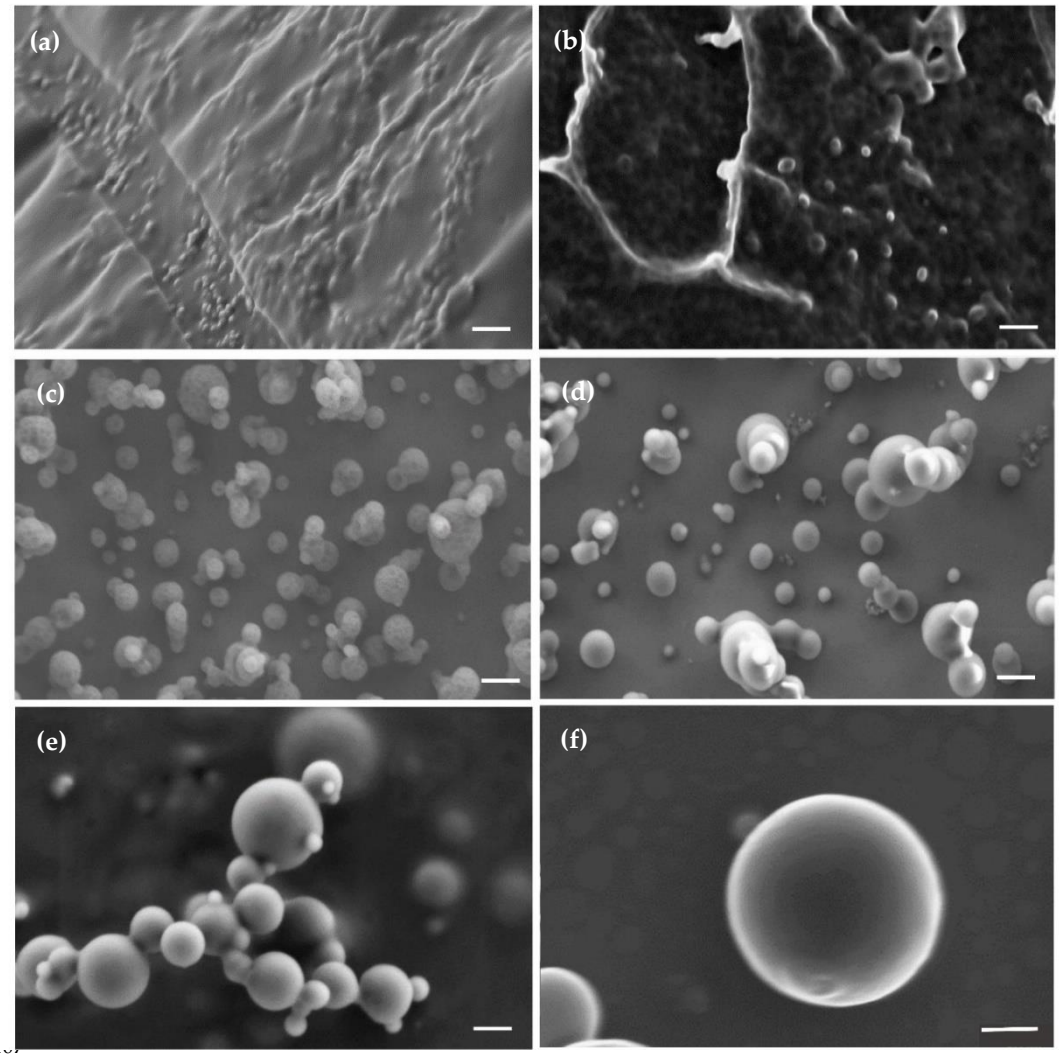

Figure 4. Representative HR-SEM micrographs of (A,B) freeze- and (C-F) spray-dried mixed polymeric micelles. (A) CBD-free non-crosslinked mixed PMs, (B) CBD-loaded non-crosslinked mixed PMs, (C) CBD-free non-crosslinked mixed PMs, (D) CBD-free crosslinked mixed PMs, (E) CBD-loaded non-crosslinked mixed PMs and (F) CBD-loaded crosslinked mixed PMs. Scale bar: 200 nm.

However, as usual after freeze-drying of nanoparticles made of polysaccharides, they formed a polymeric network in which PMs are strongly bound to each other and where they cannot be easily visualized (**Figure 4A**). No major differences were observed upon CBD encapsulation (**Figure 4B**). When the PMs were spray-dried, powders showed spherical individual particles with smooth surface (**Figure 4C-F**). Some of the particles were larger than the size measured for the PMs by DLS, NTA and cryo-TEM (up to 200 nm), and

Preprints (www.preprints.org) | NOT PEER-REVIEWED | Posted: 19 November 2021 doi:10.20944/preprints202111.0364.v1

some of them were even in the micrometer scale range. It is worth mentioning that these large particles are not the mixed PMs. Conversely, they are particles generated by the fast drying of the suspension droplets generated by the spraying head of the spray-dryer [78]. After freeze- and spray-drying, powders were resuspended in the original volume of water to render a final copolymer concentration of 0.1% w/v, and the D_h and PDI of the PMs was measured by DLS. Results are summarized in **Table 2**.

Table 2. Hydrodynamic diameter (D_h) and polydispersity index (PDI) of CBD-free and CBD-loaded mixed PMs (0.1% w/v) before and after crosslinking that were freeze- or spray-dried and redispersed in the original volume of water, as determined by DLS at 25°C.

Sample	Drying method	D_h – Intensity (nm) ± S.D.	PDI ± S.D.
Non-crosslinked mixed PMs	Freeze-drying	113 ± 2	0.33 ± 0.02
	Spray-drying	140 ± 10	0.41 ± 0.04
Crosslinked mixed PMs	Freeze-drying	139 ± 4	0.36 ± 0.01
	Spray-drying	135 ± 4	0.38 ± 0.03
CBD-loaded non-crosslinked mixed PMs	Freeze-drying	130 ± 10	0.73 ± 0.03
	Spray-drying	129 ± 6	0.30 ± 0.03
CBD-loaded crosslinked mixed PMs	Freeze-drying	155 ± 8	0.62 ± 0.03
	Spray-drying	142 ± 1	0.41 ± 0.06

The redispersion of the freeze-dried mixed PMs was inefficient, the suspension was not completely translucent, and relatively large aggregates were observed by the naked eye. Only after at least 16 h of intensive magnetic stirring, the suspension became more translucent. DLS results indicated that although the D_h did not dramatically change (generally, a growth of 10 to 20 nm of the size was observed), the PDI values increased sharply, this phenomenon being more noticeable for CBD-loaded mixed PMs (from approximately 0.20 up to 0.73), meaning that these PMs form stable aggregates upon freeze-drying (**Table 2**). Conversely, resuspensions of spray-dried PMs were translucent even after only 2-3 h of magnetic stirring and no large aggregates could be visualized with the naked eye. The D_h and PDI of these PMs remained almost unchanged and PDI values were smaller than those of freeze-dried counterparts. Based on these results, cell studies in vitro were conducted with fresh and spray-dried redispersed CBD-free and CBD-loaded mixed PMs.

3.4. Compatibility of mixed polymeric micelles with human cornea epithelial cells

Cell compatibility studies *in vitro* play a key role in the decision-making process towards preclinical and clinical research. We aimed to develop mucoadhesive CBD-loaded PMs for mucosal drug delivery by different administration routes with special interest in ocular delivery to treat eye inflammation. In this context, we evaluated the compatibility of CBD-free and CBD-loaded mixed PMs in a human cornea epithelial cell line. In this framework, cells were exposed to different fresh and spray-dried PMs (0.05%, 0.10% and 0.15% w/v)

Preprints (www.preprints.org) | NOT PEER-REVIEWED | Posted: 19 November 2021 doi:10.20944/preprints202111.0364.v1

for 4 and 24 h and the viability estimated by the MTT assay. In general, the lowest PM concentration (0.05% w/v) showed viability values >70% even after 24 h except for spray-

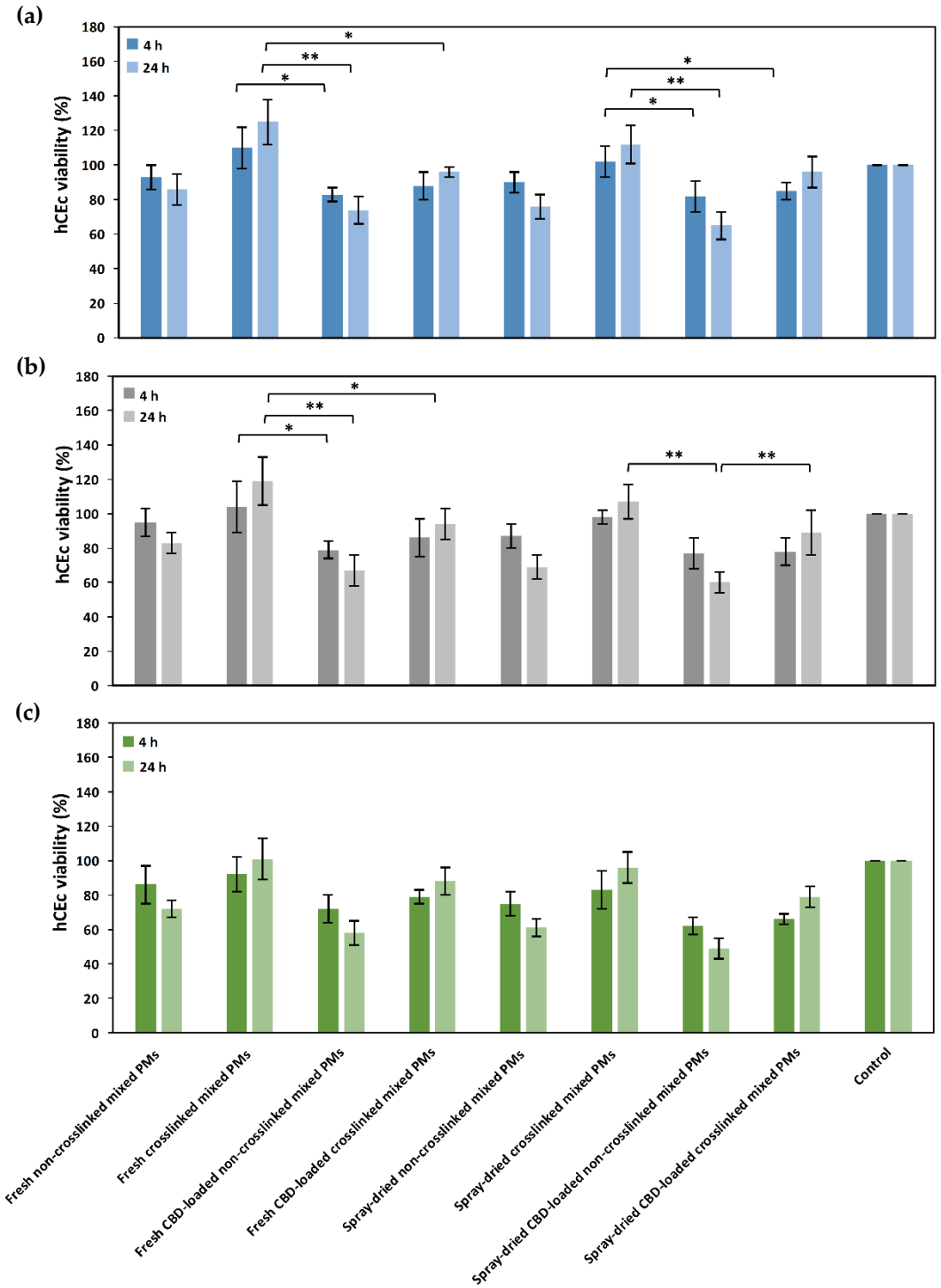

dried and redispersed CBD-loaded non-crosslinked PMs that displayed a slight decrease to 65 ± 8% after 24 h (**Figure 5A**). Cell viability values >70% comply with the guidelines of ISO 10993-5 for the evaluation of the cytotoxicity of medical devices *in vitro*. The cell viability loss increased for 0.10% w/v PMs, especially for the non-crosslinked ones due to the more positively-charged surface that contributes to cell toxicity. In contrast, crosslinked PMs showed viability values >70%, regardless of the CBD loading and the spray-drying processing (**Figure 5B**).

 doi:10.20944/preprints202111.0364.v1

Figure 5. hCEc viability upon exposure to (A) 0.05%, (B) 0.10% and (C) 0.15% w/v mixed PMs after 4 and 24 h, as estimated by the MTT assay (n = 5). Statistically significant difference ($P < 0.05$); **statistically significant difference ($P < 0.01$).

When the PM concentration increased to 0.15% w/v, the cell viability dropped more, especially for non-crosslinked samples that showed 62-72% viability, with fresh mixed PMs displaying higher viability values than the spray-dried ones (**Figure 5C**). Viability values >100% could be explained by cell stress upon exposure to the PMs, which results in a transient increase of the metabolic activity after 4 h with a decrease below 100% later (24 h). It is also worth stressing that the viability decrease between fresh and spray-dried and redispersed PMs was not statistically significant and thus, this processing method is a promising strategy to improve the physicochemical stability of the cargo and the PMs in the long-term [78]. Additionally, as discussed above, ionotropic crosslinking of CS domains in the

Preprints (www.preprints.org) | NOT PEER-REVIEWED | Posted: 19 November 2021 doi:10.20944/preprints202111.0364.v1

mixed PMs not only was meant to physically stabilize them under extreme dilution but also improved cell viability by 10-20% when compared to non-crosslinked counterparts, this phenomenon being independent of the CBD loading and the processing by spray-drying (or not). This phenomenon stems from the fact that this crosslinking pathway reduces the surface charge on the PMs and the interaction with the negatively-charged cell membrane. This trend was observed at all the PM concentrations, and particularly after 24 h. In addition, CBD consistently results in slightly lower viability values (viability decrease of ~10% after 4 h and ~20-30% after 24 h) than cells treated with unloaded PMs. The cytotoxicity CBD on human cells has been reported in the scientific literature though in most cases CBD was dissolved in a cosolvent such as ethanol or DMSO [80]. Interestingly, all 0.05% w/v and most 0.10% w/v PMs showed viability values that comply with the ISO 10993-5 guidelines (**Figure 5A,B**). Based on these findings, permeability assays with hCEc were conducted with 0.01% and 0.03% w/v PMs to ensure optimal cell viability and the monolayer integrity for at least 4 h (see below).

3.5. Permeability of mixed polymeric micelles across a model of corneal epithelium in vitro

Since the self-assembly of CS-PMMA30 and PVA-PMMA16 to form mixed PMs is random, the use of FITC-labeled PVA-PMMA16 in their preparation ensured the fluorescent labeling of all the PMs and preserved free amine groups in the sidechain of CS for ionotropic crosslinking with TPP and interaction and transient opening of tight junctions in epithelial monolayers.

First, we characterized the permeability of CBD-free crosslinked mixed PMs in a corneal epithelium model by measuring the P_{app} under LL and AL conditions [81]. For these experiments, we utilized only crosslinked 0.01% and 0.03% w/v PMs because they are prepared at a concentration (0.1% w/v) above the CMC, crosslinked and then, diluted. Since the concentrations used are below the CMC of these copolymers, non-crosslinked PMs could not be used. To estimate the integrity of hCEc monolayers, TEER values were measured over 14-21 days until a constant value between 140 and 170 $\Omega \cdot cm^2$ was measured for LL and AL conditions, respectively. It is important to stress that an increase in the TEER value of 25-30 $\Omega \cdot cm^2$ under AL incubation conditions on the same experiment day was consistent with the formation of stronger tight junctions by these epithelial cell line, which might reduce the permeability across it. This comparison is physiologically relevant because the outer cells of the human corneal epithelium are exposed to air and covered by a thin layer of mucus that preserves their hydration, what usually results in the formation of more and stronger tight junctions [81]. This behavior is like other epithelia exposed to air such as the nasal epithelium [46]. As expected, PMs systematically crossed the cell monolayer faster and the calculated P_{app} was greater for LL than for AL interface owing to the formation of stronger tight junctions by the latter model, as supported by TEER measurements (**Figure 6**). This observation was independent of the PMs (fresh or spray-dried and redispersed). For example, under LL conditions, fresh 0.03% crosslinked mixed PMs displayed P_{app} of 39 ± 7 x 10^{-7} cm/s (**Figure 6**). The same PMs under AL setup showed a P_{app} value of 24 ± 5 cm/s. Interestingly, spray-drying and redispersion led to a significant decrease of the P_{app} across hCEc monolayers when compared to fresh PMs, regardless the monolayer properties and the micellar concentration. For example, fresh 0.01% w/v crosslinked PMs under LL conditions displayed P_{app} of 24 ± 4 x 10^{-7} cm/s, while the spray-dried and redispersed counterparts of 18 ± 4 x 10^{-7} cm/s, values decreasing for AL conditions. In addition, the P_{app} was affected by the PM concentration and, in general, P_{app} values in hCEc monolayers under LL and AL conditions increased with the PM concentration, suggesting the key contribution of the paracellular pathway (**Figure 7**). Moreover, P_{app} values measured in hCEc were substantially smaller than measured for the same mixed PMs under the same conditions in *in vitro* models that mimic the intestinal epithelium (Caco-2 cell line, P_{app} of 40-110 x 10^{-7} cm/s) [82] and the nasal epithelium (RPMI 2650, P_{app} of 34-60 x 10^{-7}

Preprints (www.preprints.org) | NOT PEER-REVIEWED | Posted: 19 November 2021 doi:10.20944/preprints202111.0364.v1

cm/s) [46]. These differences in permeability *in vitro* are most probably associated with the differential ability of epithelial cells to form tight junctions [83].

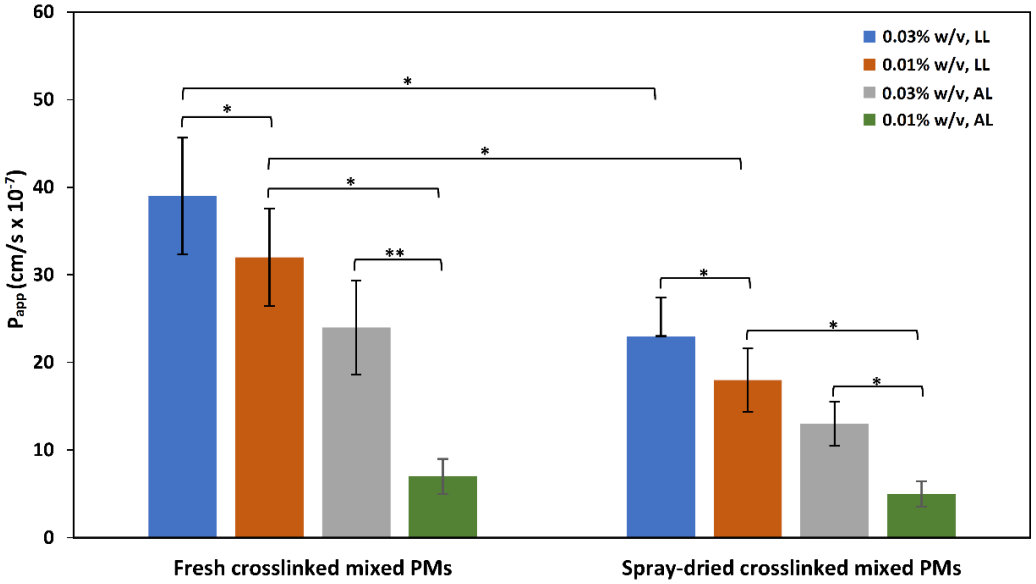

Figure 6. Apparent permeability coefficient (P_{app}) of 0.01% and 0.03% w/v CBD-free crosslinked mixed PMs in hCEc monolayers under LL and AL conditions (n = 5). *Statistically significant difference (P <0.05); **statistically significant difference (P <0.01).

At the end of each permeability study, we measured the fluorescence in both the donor and the acceptor chamber to calculate the mass balance and estimate the percentage of CBD-free mixed PMs retained by the cell monolayer due to unspecific adsorption or cell internalization, this percentage being always <12%, in good agreement with results reported elsewhere [84]. Based on this, intracellular trafficking is expected to have minimum effect on the permeability results.

After assessing the permeability of CBD-free PMs, we characterized the permeability of 0.03% w/v CBD-loaded fresh crosslinked mixed PMs containing 20% w/v CBD loading under LL and AL conditions. To evaluate the permeability of CBD encapsulated within mixed PMs, we did not label the PMs with FITC because CBD was extracted from the samples and the concentration measured by the Beam test (see above).

Results of this experiments indicated that fresh CBD-loaded crosslinked mixed PMs cross this model of corneal epithelium *in vitro*. As expected, the permeability rate under LL conditions was faster than under AL ones; e.g., at the end of the experiment (4 h), 82% and 53% of the encapsulated CBD was measured in the acceptor compartment for LL and AL setups, respectively, at the end of assay (**Figure 7**). These results of permeability rate were like those shown by unloaded PMs (data not shown) and indicated the key role played by the nanocarrier in the transport of this hydrophobic cargos across this biological barrier. The conduction of a similar permeability study with free CBD was not possible owing to its extremely low aqueous solubility (~10 μg/mL); the initial CBD concentration in the donor compartment by using the mixed PMs was 0.006% w/v (equivalent to 60 μg/mL).

Preprints (www.preprints.org) | NOT PEER-REVIEWED | Posted: 19 November 2021 doi:10.20944/preprints202111.0364.v1

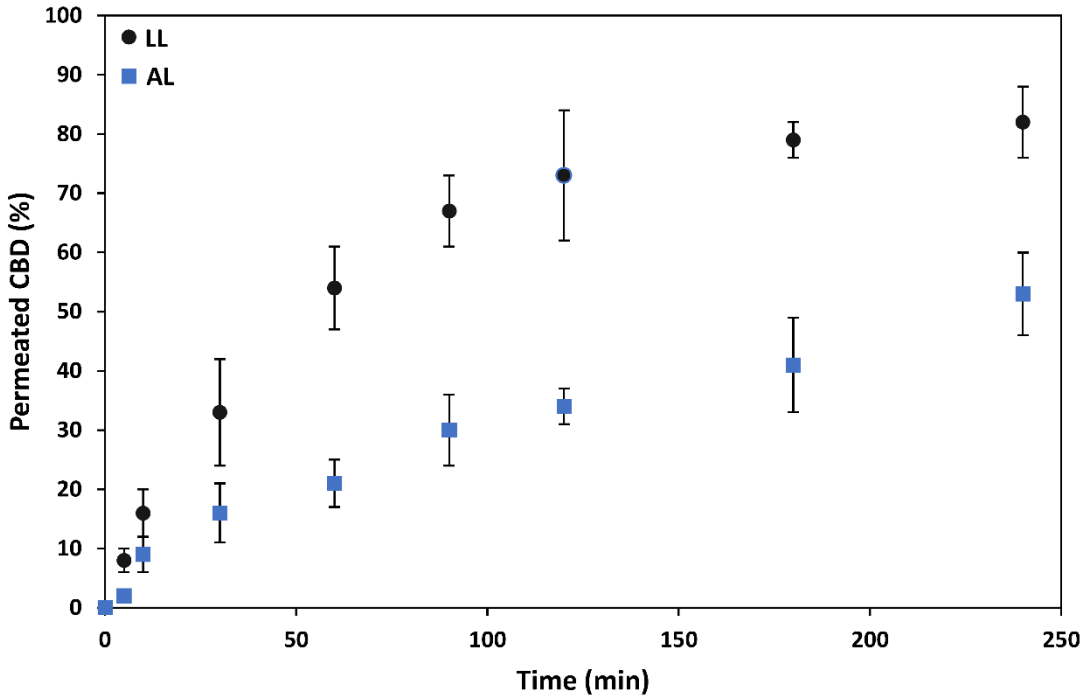

Figure 7. Permeability of 0.03% w/v CBD-loaded crosslinked mixed PMs across hCEc monolayer under LL and AL conditions (n = 3). The CBD loading in the PMs was 20% w/w and the final concentration in the donor compartment 0.006% w/v.

It is also important to stress that our model of corneal epithelium is deprived of the outer mucus layer that covers the cornea. Our PMs are mucoadhesive and this feature is expected to prolong their residence time with respect to non-mucoadhesive ones, which in turn, could increase the amount of drug delivered across the cornea over time. As mentioned above, CBD-loaded crosslinked mixed PMs are larger than the unloaded ones though still in the size range that fits trans-mucosal paracellular transport. Overall, our results support the promise of these CBD-loaded nanocarriers as a drug delivery platform to the cornea and the inner eye.

4. Conclusions

This work reports on the synthesis and characterization of mucoadhesive mixed CS-PMMA30:PVA-PMMA16 PMs (1:1 weight ratio) for the loading of CBD and trans-corneal delivery of CBD for potential application in inflammatory eye conditions. A high CBD loading of up to 20% w/w was achieved by using a simple and reproducible microfluidic system. Mixed PMs showed monomodal size and narrow size distributions with sizes in the 100-170 nm range and spherical morphology, as visualized by cryo-TEM. In addition, mixed PMs were successfully stabilized physically by non-covalent crosslinking and the size of crosslinked counterparts increase slightly though it remained <200 nm, fitting mucosal drug delivery. Then, the cell compatibility of the different PMs was evaluated by using a human corneal epithelial cell line that serves as a model of outer surface of the eye. CBD-free and CBD-loaded mixed PMs showed good cell compatibility before and after the crosslinking. Additionally, we investigated the ability of the mixed PMs to cross models of epithelium *in vitro* and measured the P_{app} of the mixed PMs in confluent hCEc monolayers under LL and AL conditions. Permeability across corneal epithelium is a crucial step to ensure efficient ocular drug delivery. Findings showed that these mixed PMs cross this corneal epithelium model even under AL conditions, at which cells form tighter tight junctions most probably by transiently opening them (paracellular mechanism). Finally, these results were supported by showing the efficient permeability of CBD across both LL

and AL models. Overall, our results support the promise of these PMs as a drug delivery platform for the treatment of eye diseases.

Author Contributions: Conceptualization, A.S.; experimental work, H.M.H. and R.B.S.; data analysis, H.M.H., R.B.S. and A.S.; writing—original draft preparation, A.S. and H.M.H.; All authors have read and agreed to the published version of the manuscript.

Funding: This work was funded by the Israel Innovation Authority (Grant NOFAR #65776). The partial support of the Russell Berrie Nanotechnology Institute (RBNI, Technion-Israel Institute of Technology) is also acknowledged.

Institutional Review Board Statement: Not applicable.

Informed Consent Statement: Not applicable.

Conflicts of Interest: The authors declare no conflicts of interest.

References

1. Larsen, C.; Shahinas, J. Dosage, Efficacy and Safety of Cannabidiol Administration in Adults: A Systematic Review of Human Trials. *J. Clin. Med. Res.* **2020**, *12*, 129–141.
2. Śledziński, P.; Zeyland, J.; Słomski, R.; Nowak, A. The current state and future perspectives of cannabinoids in cancer biology. *Cancer Med.* **2018**, *7*, 765–775.
3. Perucca, E. Cannabinoids in the Treatment of Epilepsy: Hard Evidence at Last? *J. Epilepsy Res.* **2017**, *7*.
4. Medical Cannabis Market Size, Trends & Growth | 2021 to 2026 Available online: https://www.globenewswire.com/news-release/2020/07/14/2062165/0/en/Medical-Cannabis-Market-Size-Share-Growth-Analysis-Global-Trends-Industry-Overview-Regional-Forecast-by-2027-Top-Leaders-Aurora-Cannabis-Aphria-Medical-Cannabis-MedReleaf-Corp-Medi.html.
5. Ujváry, I.; Hanuš, L. Human Metabolites of Cannabidiol: A Review on Their Formation, Biological Activity, and Relevance in Therapy. *Cannabis Cannabinoid Res.* **2016**, *1*, 90–101.
6. Bruni, N.; Pepa, C. Della; Oliaro-Bosso, S.; Pessione, E.; Gastaldi, D.; Dosio, F. Cannabinoid delivery systems for pain and inflammation treatment. *Molecules* **2018**, *23*, 2478.
7. Barchel, D.; Stolar, O.; De-Haan, T.; Ziv-Baran, T.; Saban, N.; Fuchs, D.O.; Koren, G.; Berkovitch, M. Oral cannabidiol use in children with autism spectrum disorder to treat related symptoms and Co-morbidities. *Front. Pharmacol.* **2019**, *9*, 1521.
8. Odi, R.; Bibi, D.; Wager, T.; Bialer, M. A perspective on the physicochemical and biopharmaceutic properties of marketed antiseizure drugs—From phenobarbital to cenobamate and beyond. *Epilepsia* **2020**, *61*, 1543–1552.
9. Cherniskov, I.; Izgelov, D.; Domb, A.J.; Hoffman, A. The effect of Pro NanoLipospheres (PNL) formulation containing natural absorption enhancers on the oral bioavailability of delta-9-tetrahydrocannabinol (THC) and cannabidiol (CBD) in a rat model. *Eur. J. Pharm. Sci.* **2017**, *109*, 21–30.
10. Perucca, E.; Bialer, M. Critical Aspects Affecting Cannabidiol Oral Bioavailability and Metabolic Elimination, and Related Clinical Implications. *CNS Drugs* **2020**, *34*, 795–800.
11. Millar, S.A.; Maguire, R.F.; Yates, A.S.; O'sullivan, S.E. Towards better delivery of cannabidiol (Cbd). *Pharmaceuticals* **2020**, *13*, 1–15.
12. Millar, S.A.; Stone, N.L.; Yates, A.S.; O'Sullivan, S.E. A systematic review on the pharmacokinetics of cannabidiol in humans. *Front. Pharmacol.* **2018**, *9*, 1365.
13. Adelli, G.R.; Bhagav, P.; Taskar, P.; Hingorani, T.; Pettaway, S.; Gul, W.; ElSohly, M.A.; Repka, M.A.; Majumdar, S. Development of a Δ9-tetrahydrocannabinol amino acid-dicarboxylate prodrug with improved ocular bioavailability. *Investig. Ophthalmol. Vis. Sci.* **2017**, *58*, 2167–2179.
14. Aebersold, A.; Duff, M.; Sloan, L.; Song, Z. Cannabidiol Signaling in the Eye and Its Potential as an Ocular Therapeutic Agent. *Cell. Physiol. Biochem.* **2021**, *55*, 1–14.
15. Rapino, C.; Tortolani, D.; Scipioni, L.; Maccarrone, M. Neuroprotection by (endo)Cannabinoids in Glaucoma and Retinal Neurodegenerative Diseases. *Curr. Neuropharmacol.* **2017**, *16*, 959–970.
16. Straiker, A. What is currently known about cannabidiol and ocular pressure. *Expert Rev. Ophthalmol.* **2019**, *14*, 259–261.
17. Tomida, I.; Perlwee, R.G.; Azuara-Blanco, A. Cannabinoids and glaucoma. *Br. J. Ophthalmol.* **2004**, *88*, 708–713.

18. Grotenhermen, F. Pharmacokinetics and pharmacodynamics of cannabinoids. *Clin. Pharmacokinet.* **2003**, *42*, 327–360.

19. Ahmed, I.; Patton, T.F. Importance of the noncorneal absorption route in topical ophthalmic drug delivery. *Investig. Ophthalmol. Vis. Sci.* **1985**, *26*, 584–587.

20. Davies, N.M. Biopharmaceutical considerations in topical ocular drug delivery. *Clinical and Experimental Pharmacology and Physiology* **2000**, 27, 558–562.

21. Gaudana, R.; Jwala, J.; Boddu, S.H.S.; Mitra, A.K. Recent perspectives in ocular drug delivery. *Pharm. Res.* **2009**, *26*, 1197–1216.

22. DelMonte, D.W.; Kim, T. Anatomy and physiology of the cornea. *J. Cataract Refract. Surg.* **2011**, *37*, 588–598.

23. Soares, S.; Sousa, J.; Pais, A.; Vitorino, C. Nanomedicine: Principles, properties, and regulatory issues. *Front. Chem.* **2018**, *6*, 360.

24. Anselmo, A.C.; Mitragotri, S. Nanoparticles in the clinic: An update. *Bioeng. Transl. Med.* **2019**, *4*, e10143.

25. Shi, J.; Votruba, A.R.; Farokhzad, O.C.; Langer, R. Nanotechnology in drug delivery and tissue engineering: From discovery to applications. *Nano Lett.* **2010**, *10*, 3223–3230.

26. Sosnik, A.; Mühlebach, S. Editorial: Drug Nanoparticles and Nano-Cocrystals: From Production and Characterization to Clinical Translation. *Adv. Drug Deliv. Rev.* **2018**, *131*, 1–2.

27. Sosnik, A.; Carcaboso, A.M. Nanomedicines in the future of pediatric therapy. *Adv. Drug Deliv. Rev.* **2014**, *73*, 140–161.

28. Imperiale, J.C.; Acosta, G.B.; Sosnik, A. Polymer-based carriers for ophthalmic drug delivery. *J. Control. Release* **2018**, *285*, 106–141.

29. Sosnik, A.; Das Neves, J.; Sarmento, B. Mucoadhesive polymers in the design of nano-drug delivery systems for administration by non-parenteral routes: A review. *Prog. Polym. Sci.* **2014**, *39*, 2030–2075.

30. Ghezzi, M.; Pescina, S.; Padula, C.; Santi, P.; Del Favero, E.; Cantù, L.; Nicoli, S. Polymeric micelles in drug delivery: An insight of the techniques for their characterization and assessment in biorelevant conditions. *J. Control. Release* **2021**, *332*, 312–336.

31. Torchilin, V.P. Micellar nanocarriers: Pharmaceutical perspectives. *Pharm. Res.* **2007**, *24*, 1–16.

32. Sosnik, A. Temperature- and pH-sensitive polymeric micelles for drug encapsulation, release and targeting. *RSC Smart Mater.* **2013**, *1*, 115–147.

33. Chiappetta, D.A.; Sosnik, A. Poly(ethylene oxide)-poly(propylene oxide) block copolymer micelles as drug delivery agents: Improved hydrosolubility, stability and bioavailability of drugs. *Eur. J. Pharm. Biopharm.* **2007**, *66*, 303–317.

34. Moretton, M.A.; Glisoni, R.J.; Chiappetta, D.A.; Sosnik, A. Molecular implications in the nanoencapsulation of the anti-tuberculosis drug rifampicin within flower-like polymeric micelles. *Colloids Surfaces B Biointerfaces* **2010**, *79*, 467–479.

35. Raskin, M.M.; Schlachet, I.; Sosnik, A. Mucoadhesive nanogels by ionotropic crosslinking of chitosan-g-oligo(NiPAam) polymeric micelles as novel drug nanocarriers. *Nanomedicine* **2016**, *11*, 217–233.

36. Mahmud, A.; Xiong, X.B.; Aliabadi, H.M.; Lavasanifar, A. Polymeric micelles for drug targeting. *J. Drug Target.*

2007, *15*, 553–584.

37. Chiappetta, D.A.; Hocht, C.; Taira, C.; Sosnik, A. Efavirenz-loaded polymeric micelles for pediatric anti-HIV pharmacotherapy with significantly higher oral bioavailaibility. *Nanomedicine* **2010**, *5*, 11–23.

38. Ribeiro, A.; Sosnik, A.; Chiappetta, D.A.; Veiga, F.; Concheiro, A.; Alvarez-Lorenzo, C. Single and mixed poloxamine micelles as nanocarriers for solubilization and sustained release of ethoxzolamide for topical glaucoma therapy. *J. R. Soc. Interface* **2012**, *9*, 2059–2069.

39. Chiappetta, D.A.; Hocht, C.; Opezzo, J.A.W.; Sosnik, A. Intranasal administration of antiretroviral-loaded micelles for anatomical targeting to the brain in HIV. *Nanomedicine* **2013**, *8*, 223–237.

40. Sosnik, A.; Menaker Raskin, M. Polymeric micelles in mucosal drug delivery: Challenges towards clinical translation. *Biotechnol. Adv.* **2015**, *33*, 1380–1392.

41. Glisoni, R.J.; Quintana L, S.S.; Molina, M.; Calderón, M.; Moglioni, A.G.; Sosnik, A. Chitosan-g-oligo(epsilon-caprolactone) polymeric micelles: Microwave-assisted synthesis and physicochemical and cytocompatibility characterization. *J. Mater. Chem. B* **2015**, *3*, 4853–4864.

42. Moshe, H.; Davizon, Y.; Menaker Raskin, M.; Sosnik, A. Novel poly(vinyl alcohol)-based amphiphilic nanogels by non-covalent boric acid crosslinking of polymeric micelles. *Biomater. Sci.* **2017**, *5*, 2295–2309.

43. Noi, I.; Schlachet, I.; Kumarasamy, M.; Sosnik, A. Permeability of novel chitosan-g-Poly(methyl methacrylate) amphiphilic nanoparticles in a model of small intestine in vitro. *Polymers (Basel).* **2018**, *10*, 478.

44. Schlachet, I.; Trousil, J.; Rak, D.; Knudsen, K.D.; Pavlova, E.; Nyström, B.; Sosnik, A. Chitosan-graft-poly(methyl methacrylate) amphiphilic nanoparticles: Self-association and physicochemical characterization. *Carbohydr. Polym.* **2019**, *212*, 412–420.

45. Moshe Halamish, H.; Trousil, J.; Rak, D.; Knudsen, K.D.; Pavlova, E.; Nyström, B.; Štěpánek, P.; Sosnik, A. Self-assembly and nanostructure of poly(vinyl alcohol)-graft-poly(methyl methacrylate) amphiphilic nanoparticles. *J. Colloid Interface Sci.* **2019**, *553*, 512–523.

46. Schlachet, I.; Sosnik, A. Mixed Mucoadhesive Amphiphilic Polymeric Nanoparticles Cross a Model of Nasal Septum Epithelium in Vitro. *ACS Appl. Mater. Interfaces* **2019**, *11*, 21360–21371.

47. Sverdlov Arzi, R.; Kay, A.; Raychman, Y.; Sosnik, A. Excipient-free pure drug nanoparticles fabricated by microfluidic hydrodynamic focusing. *Pharmaceutics* **2021**, *13*, 1–20.

48. Pourseyed Lazarjani, M.; Torres, S.; Hooker, T.; Fowlie, C.; Young, O.; Seyfoddin, A. Methods for quantification of cannabinoids: a narrative review. *J. Cannabis Res.* **2020**, *2*.

49. Preedy, V.R. *Handbook of Cannabis and Related Pathologies*; **2017**; ISBN 9780128007563.

50. Toropainen, E.; Ranta, V.P.; Talvitte, A.; Suhonen, P.; Urtti, A. Culture model of human corneal epithelium for prediction of ocular drug absorption. *Investig. Ophthalmol. Vis. Sci.* **2001**, *42*, 2942–2948.

51. Sogias, I.A.; Williams, A.C.; Khutoryanskiy, V. V. Why is chitosan mucoadhesive? *Biomacromolecules* **2008**, *9*, 1837–1842.

52. Silva, M.M.; Calado, R.; Marto, J.; Bettencourt, A.; Almeida, A.J.; Gonçalves, L.M.D. Chitosan nanoparticles as a mucoadhesive drug delivery system for ocular administration. *Mar. Drugs* **2017**, *15*, 370.

53. Zamboulis, A.; Nanaki, S.; Michailidou, G.; Koumentakou, I.; Lazaridou, M.; Ainali, N.M.; Xanthopoulou, E.;

Bikiaris, D.N. Chitosan and its derivatives for ocular delivery formulations: Recent advances and developments. *Polymers (Basel).* **2020**, *12*, 1519.

54. Thanou, M.; Verhoef, J.C.; Junginger, H.E. Chitosan and its derivatives as intestinal absorption enhancers. *Advanced Drug Delivery Reviews* 2001, 50, S91–S101.

55. Janagam, D.R.; Wu, L.; Lowe, T.L. Nanoparticles for drug delivery to the anterior segment of the eye. *Adv. Drug Deliv. Rev.* **2017**, *122*, 31–64.

56. Nepp, J.; Knoetzl, W.; Prinz, A.; Hoeller, S.; Prinz, M. Management of moderate-to-severe dry eye disease using chitosan-N-acetylcysteine (Lacrimera®) eye drops: a retrospective case series. *Int. Ophthalmol.* **2020**, *40*, 1547–1552.

57. Pepić, I.; Lovrić, J.; Filipović-Grčić, J. How do polymeric micelles cross epithelial barriers? *Eur. J. Pharm. Sci.* **2013**, *50*, 42–55.

58. Kong, X.; Xu, W. Biodegradation and biocompatibility of a degradable chitosan vascular prosthesis. *Int. J. Clin. Exp. Med.* **2015**, *8*, 3498–3505.

59. Paradossi, G.; Cavalieri, F.; Chiessi, E.; Spagnoli, C.; Cowman, M.K. Poly(vinyl alcohol) as versatile biomaterial for potential biomedical applications. *Journal of Materials Science: Materials in Medicine* **2003**, 14, 687–691.

60. Nafee, N.A.; Boraie, N.A.; Ismail, F.A.; Mortada, L.M. Design and characterization of mucoadhesive buccal patches containing cetylpyridinium chloride. *Acta Pharm.* **2003**, *53*, 199–212.

61. Gao, W.; Lai, J.C.K.; Leung, S.W. Functional enhancement of chitosan and nanoparticles in cell culture, tissue engineering, and pharmaceutical applications. *Front. Physiol.* **2012**, *3 AUG*, 321.

62. Huang, M.; Khor, E.; Lim, L.Y. Uptake and Cytotoxicity of Chitosan Molecules and Nanoparticles: Effects of Molecular Weight and Degree of Deacetylation. *Pharm. Res.* **2004**, *21*, 344–353.

63. Schlachet, I. Innovative nano-biomaterials for the improved delivery of antitumorals to the central nervous system in the therapy of pediatric brain tumors. *PhD thesis*, Technion-Israel Institute of Technology, **2019**.

64. Bettencourt, A.; Almeida, A.J. Poly(methyl methacrylate) particulate carriers in drug delivery. *J. Microencapsul.* **2012**, *29*, 353–367.

65. Shaked, E.; Shani, Y.; Zilberman, M.; Scheinowitz, M. Poly(methyl methacrylate) particles for local drug delivery using shock wave lithotripsy: In vitro proof of concept experiment. *J. Biomed. Mater. Res. - Part B Appl. Biomater.* **2015**, *103*, 1228–1237.

66. Gozum, N.; Safgonul Unal, E.; Altan-Yaycioglu, R.; Gucukoglu, A.; Ozgun, C. Visual performance of acrylic and PMMA intraocular lenses. *Eye* **2003**, *17*, 238–242.

67. Frazer, R.Q.; Byron, R.T.; Osborne, P.B.; West, K.P. PMMA: An essential material in medicine and dentistry. *J. Long. Term. Eff. Med. Implants* **2005**, *15*, 629–639.

68. Vaishya, R.; Chauhan, M.; Vaish, A. Bone cement. *J. Clin. Orthop. Trauma* **2013**, *4*, 157–163.

69. Inoue, T.; Chen, G.; Nakamae, K.; Hoffman, A.S. An AB block copolymer of oligo(methyl methacrylate) and poly(acrylic acid) for micellar delivery of hydrophobic drugs. *J. Control. Release* **1998**, *51*, 221–229.

70. Shantha, K.L.; Harding, D.R.K. Synthesis and characterisation of chemically modified chitosan microspheres. *Carbohydr. Polym.* **2002**, *48*, 247–253.

71. Reguieg, F.; Ricci, L.; Bouyacoub, N.; Belbachir, M.; Bertoldo, M. Thermal characterization by DSC and TGA analyses of PVA hydrogels with organic and sodium MMT. *Polym. Bull.* **2020**, *77*, 929–948.

72. Gaucher, G.; Dufresne, M.H.; Sant, V.P.; Kang, N.; Maysinger, D.; Leroux, J.C. Block copolymer micelles: Preparation, characterization and application in drug delivery. *Journal of Controlled Release* **2005**, 109, 169–188.

73. Kim, A.; Ng, W.B.; Bernt, W.; Cho, N.J. Validation of Size Estimation of Nanoparticle Tracking Analysis on Polydisperse Macromolecule Assembly. *Sci. Rep.* **2019**, *9*, 1–14.

74. Mazzetti, C.; Ferri, E.; Pozzi, M.; Labra, M. Quantification of the content of cannabinol in commercially available e-liquids and studies on their thermal and photo-stability. *Sci. Rep.* **2020**, *10*, 1–6.

75. Calvi, L.; Pentimalli, D.; Panseri, S.; Giupponi, L.; Gelmini, F.; Beretta, G.; Vitali, D.; Bruno, M.; Zilio, E.; Pavlovic, R.; et al. Comprehensive quality evaluation of medical Cannabis sativa L. inflorescence and macerated oils based on HS-SPME coupled to GC–MS and LC-HRMS (q-exactive orbitrap®) approach. *J. Pharm. Biomed. Anal.* **2018**, *150*, 208–219.

76. Citti, C.; Russo, F.; Linciano, P.; Strallhofer, S.S.; Tolomeo, F.; Forni, F.; Vandelli, M.A.; Gigli, G.; Cannazza, G. Origin of Δ9-tetrahydrocannabinol impurity in synthetic cannabidiol. *Cannabis Cannabinoid Res.* **2021**, *6*, 28–39.

77. Lodzki, M.; Godin, B.; Rakou, L.; Mechoulam, R.; Gallily, R.; Touitou, E. Cannabidiol - Transdermal delivery and anti-inflammatory effect in a murine model. *J. Control. Release* **2003**, *93*, 377–387.

78. Sosnik, A.; Seremeta, K.P. Advantages and challenges of the spray-drying technology for the production of pure drug particles and drug-loaded polymeric carriers. *Adv. Colloid Interface Sci.* **2015**, *223*, 40–54.

79. Abdelwahed, W.; Degobert, G.; Stainmesse, S.; Fessi, H. Freeze-drying of nanoparticles: Formulation, process and storage considerations. *Adv. Drug Deliv. Rev.* **2006**, *58*, 1688–1713.

80. Pagano, S.; Coniglio, M.; Valenti, C.; Federici, M.I.; Lombardo, G.; Cianetti, S.; Marinucci, L. Biological effects of Cannabidiol on normal human healthy cell populations: Systematic review of the literature. *Biomed. Pharmacother.* **2020**, *132*, 110728.

81. Chang, J.-E.; Basu, S.K.; Lee, V.H.L. Air-Interface Condition Promotes the Formation of Tight Corneal Epithelial Cell Layers for Drug Transport Studies. *Pharm. Res. 2000 176* **2000**, *17*, 670–676.

82. Ben Shabo, R. Mucoadhesive amphiphilic polymeric micelles for ocular drug delivery. *Msc thesis*, Technion-Israel Institute of Technology, **2021**.

83. Anderson, J.M. Molecular structure of tight junctions and their role in epithelial transport. *News Physiol. Sci.* **2001**, *16*, 126–130.

84. Schlachet, I.; Sosnik, A. Protoporphyrin IX-modified chitosan-: G -oligo(NiPAAm) polymeric micelles: From physical stabilization to permeability characterization in vitro. *Biomater. Sci.* **2017**, *5*, 128–140.